water

MDPI

Article

The Predictability of the 30 October 2020 İzmir-Samos Tsunami Hydrodynamics and Enhancement of Its Early Warning Time by LSTM Deep Learning Network

Ali Rıza Alan [1,*], Cihan Bayındır [1,2,*], Fatih Ozaydin [3] and Azmi Ali Altintas [4]

[1] Engineering Faculty, İstanbul Technical University, İstanbul 34469, Turkey
[2] Engineering Faculty, Boğaziçi University, İstanbul 34342, Turkey
[3] Institute for International Strategy, Tokyo International University, 4-42-31 Higashi-Ikebukuro, Toshima-ku, Tokyo 170-0013, Japan; fatih@tiu.ac.jp
[4] Department of Physics, Faculty of Science, İstanbul University, Vezneciler, İstanbul 34116, Turkey; azmi.altintas@istanbul.edu.tr
* Correspondence: alan21@itu.edu.tr (A.R.A.); cbayindir@itu.edu.tr (C.B.)

Abstract: Although tsunamis occur less frequently compared to some other natural disasters, they can be extremely devastating in the nearshore environment if they occur. An earthquake of magnitude 6.9 Mw occurred on 30 October 2020 at 12:51 p.m. UTC (2:51 p.m. GMT+03:00) and its epicenter was approximately 23 km south of İzmir province of Turkey, off the Greek island of Samos. The tsunami event triggered by this earthquake is known as the 30 October 2020 İzmir-Samos (Aegean) tsunami, and in this paper, we study the hydrodynamics of this tsunami using some of these artificial intelligence (AI) techniques applied to observational data. More specifically, we use the tsunami time series acquired from the UNESCO data portal at different stations of Bodrum, Syros, Kos, and Kos Marina. Then, we investigate the usage and shortcomings of the Long Short Term Memory (LSTM) DL technique for the prediction of the tsunami time series and its Fourier spectra. More specifically we study the predictability of the offshore water surface elevation dynamics, their spectral frequency and amplitude features, possible prediction success and enhancement of the accurate early prediction time scales. The uses and applicability of our findings and possible research directions are also discussed.

Keywords: 30 October 2020 İzmir-Samos (Aegean) tsunami; deep learning; LSTM; time series analysis and prediction

Citation: Alan, A.R.; Bayındır, C.; Ozaydin, F.; Altintas, A.A. The Predictability of the 30 October 2020 İzmir-Samos Tsunami Hydrodynamics and Enhancement of Its Early Warning Time by LSTM Deep Learning Network. *Water* **2023**, *15*, 4195. https://doi.org/10.3390/w15234195

Academic Editors: Helena M. Ramos, Wencheng Guo and Georg Umgiesser

Received: 6 November 2023
Revised: 25 November 2023
Accepted: 30 November 2023
Published: 4 December 2023

1. Introduction

Tsunamis are defined as surface water waves that can have a long-range and reach thousands of kilometers from their source [1,2]. They are destructive since their energy is concentrated close to a front moving at the maximum group velocity $\sqrt{gh}$, where h (considered to be constant) is the water depth [3]. Tsunamis may occur with a displacement of the water column due to reasons such as earthquakes, submarine or atmospheric events, volcanic eruptions, etc. [4]. Throughout history, there has been great material damage and loss of life due to tsunamis in coastal and inland regions [1]. Tsunamis, like other natural disasters, are natural events that are almost impossible to prevent, but whose effects can be minimized with some scientific studies. There are many studies in the literature on this subject. To assess the changes in land use and land cover brought on by the great East Japan earthquake disaster in 2011, a precise land use and land cover map for the years 2013 to 2015 post-disaster with a 30-m spatial resolution is generated in [5]. An analysis of assessing and mapping the geographical and temporal consequences of the tsunami on land use and land cover, as well as the availability of associated ecosystem services in the Thai province of Phang Nga is presented in [6]. On an approximately 4.5 km shore-normal section on

the shoreline region around Sendai, Japan; erosion, deposition, and related alterations to the landscape are established as a result of the Tohoku-oki tsunami in 2011 in [7]. The effects of a large tsunami on a low-lying coastal area in eastern Japan are determined using a mix of time-series satellite images, aerial videos, and observation from the ground; and an analysis is made between a shoreline with armored barriers and one without in [8]. The potential use of compressive sensing for the accurate measurement and modeling of the tsunami parameters, namely, water surface fluctuation, velocity, and wave pressures are examined in [9]. Despite being examined for tsunami disasters quite a lot of times with traditional observation methods such as satellite imaging, newer and technological methods have been preferred due to the inadequacy of the old methods and the demands for more detailed and useful results. For example, remote sensing is a technique that makes it possible to map and evaluate regions damaged or likely to be damaged by tsunami using satellite images [10]. Because of the large size of tsunami impact areas, recent developments in remote sensing and associated application technologies have made it feasible to use remotely sensed image data for mapping catastrophe damage distribution and determining an area's risk [11]. Another recent tsunami event took place on 30 October 2020 at 12:51 p.m. UTC (2:51 p.m. GMT+03:00) after an earthquake of 6.9 Mw, and this event is investigated by some field surveys such as [12]. Although the magnitude of the earthquake and the resulting 30 October 2020 İzmir-Samos (Aegean) tsunami flood characteristics such as the tsunami height and maximum runup are not among the most devastating ones on the earth, it was a remarkable milestone for the coastal communities along the Turkish coast of İzmir, especially at the town of Sığacık [12] due to its catastrophic consequences. The 30 October 2020 İzmir-Samos (Aegean) tsunami and its effect on various surrounding regions became and attraction of research in the recent years and many other field surveys and studies are given in the literature. For example the another field survey is conducted at the Samos island is presented in [13]. Relative sea level changes and morphotectonic implications triggered by the tsunami event is analyzed in [14]. A statistical and criticality analysis of the lower ionosphere prior to the earthquake event in performed in [15].

On the other hand, some applications of AI for tsunami data analysis are proposed in the literature. Real-time prediction of tsunami magnitudes in Osaka Bay, Japan is performed using an artificial neural network in [16]. An inverse modeling technique for the estimation of tsunami characteristics from deposits using a deep-learning neural network is studied in [17]. Early warning of tsunami inundation using convolutional neural networks and some other machine learning algorithms is analyzed in some studies such as [18–20]. In another paper, coastal tsunami prediction based on S-net observations using artificial neural network for the Tohoku, Japan is studied [21].

As one of the very successful DL networks, LSTM attracted some attention for tsunami disaster applications only very recently [22–24]. The performance of the LSTM, bi-directional LSTM and convolutional neural network–LSTM networks in predicting mean lower low water levels are analyzed in [22] where the data of two specific events recorded in Arkansas and New England/Maryland are used. The performance of recurrent neural network vs LSTM and gated recurrent units are studied in [23] where synthetic tsunami data is used. The spatiotemporal extrapolation of population data in areas prone to earthquakes and tsunamis in Lima, Peru are analyzed in [24].

This paper aims to examine the hydrodynamic characteristics and the predictability of the 30 October 2020 İzmir-Samos tsunami by using the LSTM DL network applied to data acquired using in situ and remote sensing techniques. For this purpose, we examine the prediction of the tsunami water surface fluctuation time series at different stations obtained by pressure gauges and radar and discuss their predictability using the LSTM deep learning network. We discuss the time series dynamics, root-mean-square-error (RMSE), and the spectral features of the predictions that are obtained by FFT routines. We also investigate the effect of the training data set on the performance of tsunami time series prediction both in the time as well as the spectral domain. Possible enhancement of the early warnings and early warning time scales are also discussed.

2. Methodology

2.1. Study Area

On 30 October 2020 at 12:51 p.m. UTC, an earthquake with a moment magnitude of 6.9 Mw with its epicenter off the Greek island of Samos, approximately 23 km south of İzmir occurred [25–27]. The analysis carried after the kinematic rupture process of the earthquake indicated the cascaded rupture of two fault planes, with slightly rotated strike angles, and dominated by normal faulting and oblique faulting, respectively [27]. Not only seismic and geodetic but also tsunami data was used to analyze earthquake characteristics [27]. The seismicity map shown in Figure 1 indicates the epicenter of the earthquake and the locations of 5068 aftershocks recorded on that day [28]. The earthquake's epicenter is located on the İzmir-Balikesir Transfer Zone, which extends down to Samos Island [27]. The primary seismogenic fault of the 2020 Samos earthquake is considered to be the Kaystrios Fault [27]. Kaystrios Fault along with Ikaria, Fourni, and Pythagorio Faults in the vicinity, compose a complex fault system [27]. Although the magnitude of this earthquake and the resulting 30 October 2020 İzmir-Samos (Aegean) Tsunami was not very big compared to their counterparts observed on other places on Earth, it was a major event and was of critical importance to the region. The tsunami triggered by the earthquake caused significant inundation and damage along the Turkish coastal town of Sığacık.

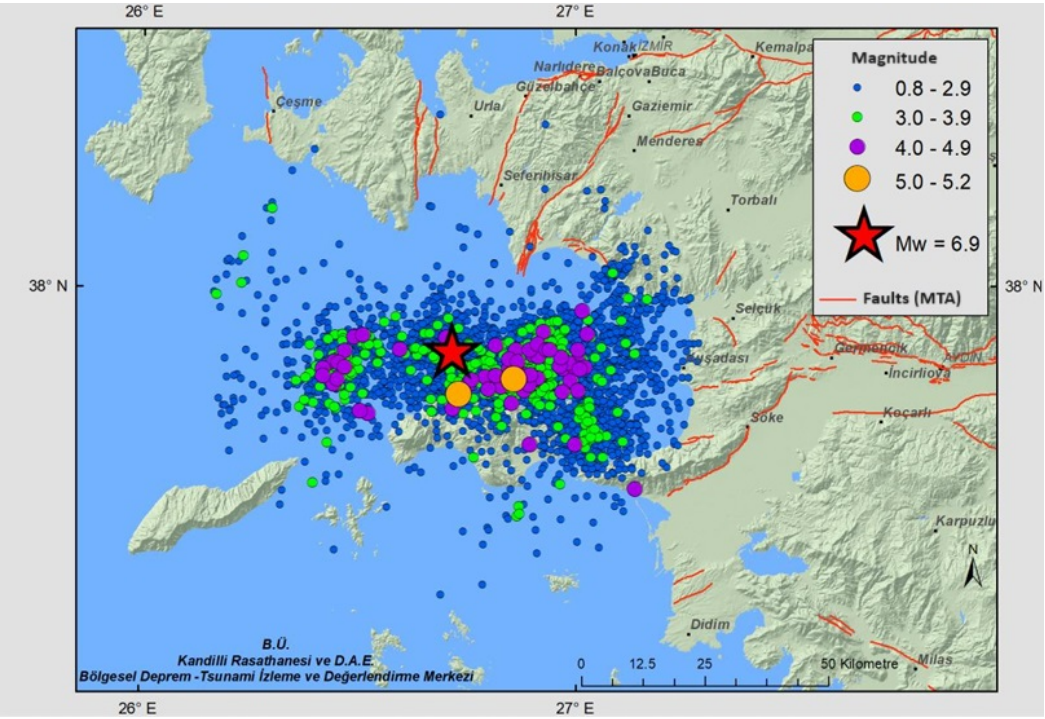

Figure 1. 30 October 2020 İzmir-Samos Earthquake seismicity map [28] (Figure courtesy of KOERI and permission to reuse of this figure is obtained from Prof. Dr. Doğan Kalafat).

The study map of the 30 October 2020 İzmir-Samos tsunami, with its earthquake epicenter and surrounding UNESCO tsunami observation stations, is depicted in Figure 2. As the figure depicts, the closest UNESCO stations are located at Bodrum, Syros, Kos, and Kos Marina [29]. The time series data used in this study are downloaded from the UNESCO website at https://www.ioc-sealevelmonitoring.org/map.php (accessed on 29 November 2023) and it is publicly available.

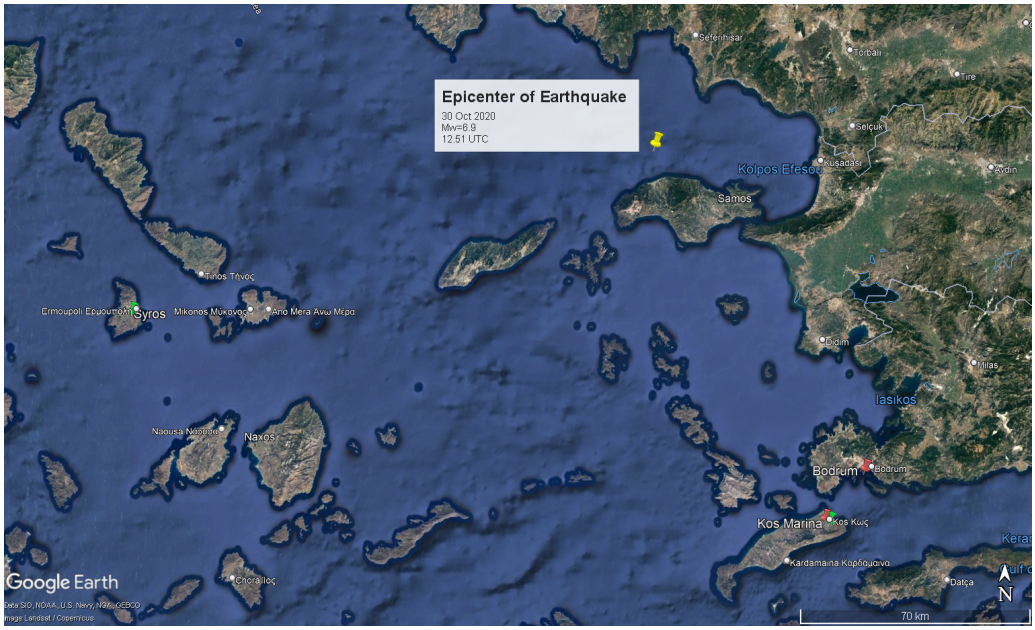

Figure 2. 30 October 2020 İzmir-Samos earthquake epicenter and surrounding UNESCO tsunami observation stations: Bodrum, Syros, Kos and Kos Marina [29].

Daily data from 30 October 2020-00:00 a.m. to 31 October 2020-00:00 a.m. UTC are obtained from all of the 4 stations mentioned above. It is useful to mention that the sampling time at the Bodrum Station is 0.5 min, whereas the sampling time for all remaining 3 stations are all 1 min. The recordings at the Bodrum Station and Syros Station are acquired by an acoustic echo sounder and a pressure gauge, respectively. The recordings at the Kos and Kos Marina Stations are acquired by radar.

The predictability of the tsunami event, its dynamics, and spectral features is the subject of this paper. More specifically, one of the very successful time series prediction tools of DL is the LSTM network, and it is studied as a possible candidate for the successful prediction of 30 October 2020 İzmir-Samos tsunami hydrodynamics. In the next section, we give a brief review of the LSTM network, and in further sections, we analyze the predictability of the 30 October 2020 İzmir-Samos tsunami using the LSTM DL network.

2.2. Review of the LSTM

Recurrent neural networks (RNN) which remain the most effective deep learning algorithms were created in the 1980s [30,31]. Forecasts can be made utilizing sequential data sets using RNN. One of those neural networks is the LSTM, and its structure is shown in Figure 3 [30,31].

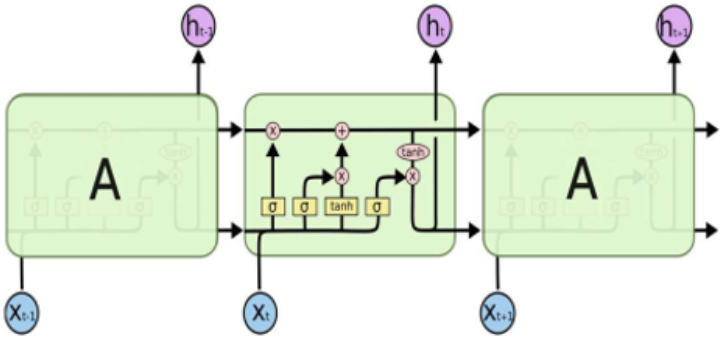

Figure 3. LSTM network structure indicating input and output times series, gates and activation functions [31].

Up to the present, numerous studies include the utilization of RNN to analyze time series [30,31]. Nevertheless, if long data sets are being used it is known that gradient disappearance or gradient burst cases take place [30,31]. LSTM architecture was first developed in 1997 to overcome these problems [30]. Data flow is provided simply thanks to the forget gate, input gate, and output gate and additionally the memory cell outside of the input, which decides that the information will be forgotten, retained, and transferred [30,31]. The mathematical formulations of these gates reads:

(a) Forget Gate:

$$f_i^{(t)} = \sigma(b_i^f + \sum_y U_{i,j}^f x_j^{(t)} + \sum_y W_{i,j} h_j^{(t-1)}), \quad (1)$$

(b) State Unit:

$$s_i^{(t)} = f_i^{(t)} s_i^{(t-1)} + g_i^t \sigma(b_i^f + \sum_y U_i x_j^{(t)} + \sum_y W_i h_j^{(t-1)}), \quad (2)$$

(c) Input Gate:

$$g_i^{(t)} = \sigma(b_i^g + \sum_y U_i^g x_j^{(t)} + \sum_y W_i^g h_j^{(t-1)}), \quad (3)$$

(d) Output Gate:

$$q_i^{(t)} = \sigma(b_i^o + \sum_y U_{i,j}^o x_j^{(t)} + \sum_y W_{i,}^o h_j^{(t-1)}), \quad (4)$$

(e) The Output:

$$h_i^{(t)} = q_i^{(t)} tanh(s_i^{(t)}), \quad (5)$$

In these formulations bias values in the input, output, and forget gates are represented as b_i^f, b_i^g, b_i^o [30,31]. The input weights belonging to the gates are shown as $U_{i,j}^f$, $U_{i,j}^g$, $U_{i,j}^o$, $U_{i,j}$ [30,31]. The recurrent weights of the gate to which they belong to are denoted as $W_{i,j}^f$, $W_{i,j}^g$, $W_{i,j}^o$, $W_{i,j}$. The letter A indicates a chunk of the deep neural net. The input time series is shown as X parameter [30,31]. In all of our simulations we use 250 epochs with 1 iteration per epoch. The learning rate is selected to be 0.001 and the learning rate schedule is piecewise. A detailed discussion and analysis of the LSTM network and its applications can be seen in [30,31]. While it can be used for many different purposes including but not limited to speech and image recognition, and retrieval of transfer functions in systems theory, we use LSTM as a tsunami time series analysis tool in this study.

3. Results and Discussion

The data used in this study is downloaded from the UNESCO website mentioned above, and it is de-tided using a spectral approach to filter out the astronomical tidal effect. For this purpose, after zeroing out the mean, an FFT-IFFT procedure is used. The water surface fluctuation spectra are obtained via FFT, and the spectral amplitudes corresponding to central frequencies between ±1% frequencies around central frequency 0 giving approximately $[-3 \times 10^{-4}$ Hz, 3×10^{-4} Hz] are zero-padded. Then, this filtered spectrum is inverted using an IFFT routine to construct the de-tided tsunami water surface fluctuation time series. The de-tided water surface fluctuation indicates a tsunami wave height on the order of approximately 8 cm at Bodrum station which is located at [latitude: 37.03217, longitude: 27.423453]; and is sheltered by mainland and islands. The de-tided water surface fluctuation, its prediction by the LSTM network, and RMSE error between observations and predictions are depicted in Figure 4. The 70% of the daily data set recorded at the Bodrum station is used as the training set, thus the training data set not only includes the pre-tsunami but also some of the post-tsunami recordings. The computation time for

this data set is 63.93 s, whereas the computation time of the LSTM DL network is 52.00 s. These times are measured on a personal machine with an Intel Core i5 processor with 16 GB RAM and 512 GB SSD. The computation times for other data sets analyzed throughout this study are similar.

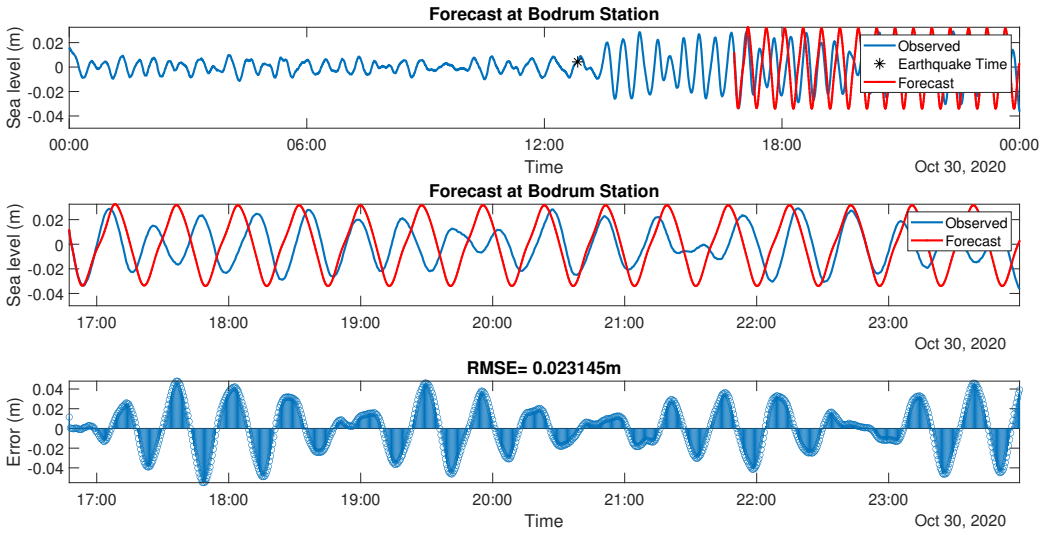

Figure 4. Time series of the İzmir-Samos tsunami water surface fluctuation recorded at Bodrum station [29] on 30 October 2020 and its prediction by LSTM DL network-without updates.

As shown in the figure, the predictions performed by LSTM can resolve the cyclic behavior. However, some shifts are present in the angular frequency of the oscillations compared to the actual recordings. The amplitude of the predictions is a better match for this data set compared to the frequencies. When an LSTM network with no updates is used, it means that only the training data set determines the success of predictions, thus actual recordings after predictions do not affect the further predictions. However, when an updated LSTM network is used, the predictions are updated according to the actual recordings of the prediction phase, thus the prediction time reduces to a one-time step. For the Bodrum Station data, this time step is 0.5 min. The results of the LSTM predictions with updates are depicted in Figure 5.

As these figures confirm, the LSTM network with updates is much more successful in predicting the Bodrum station data in terms of matching the waveform of the oscillations of the water surface fluctuations, and the RMSE is significantly enhanced compared to the not-updated case. For the majority of the time series investigated in this paper, we observe a similar tendency, however, some exceptions can also be observed. To better visualize the matching of the time series of predictions with the time series of observations, again we employ a spectral approach and obtain the Fourier spectrum via FFT routines. The spectra of the predictions for not-updated and updated cases are depicted in Figure 6.

Next, we repeat a similar analysis for the next station, which is Syros station located at [latitude: 37.438, longitude: 24.9411]. Compared to the Bodrum stations, Syros station is more prone to tsunami inundation since it is less sheltered by some islands as the station location map confirms. Thus, the tsunami wave height observed from the de-tided water surface fluctuation time series depicted in Figure 7 is larger compared to its Bodrum counterpart, being approximately 0.17 cm.

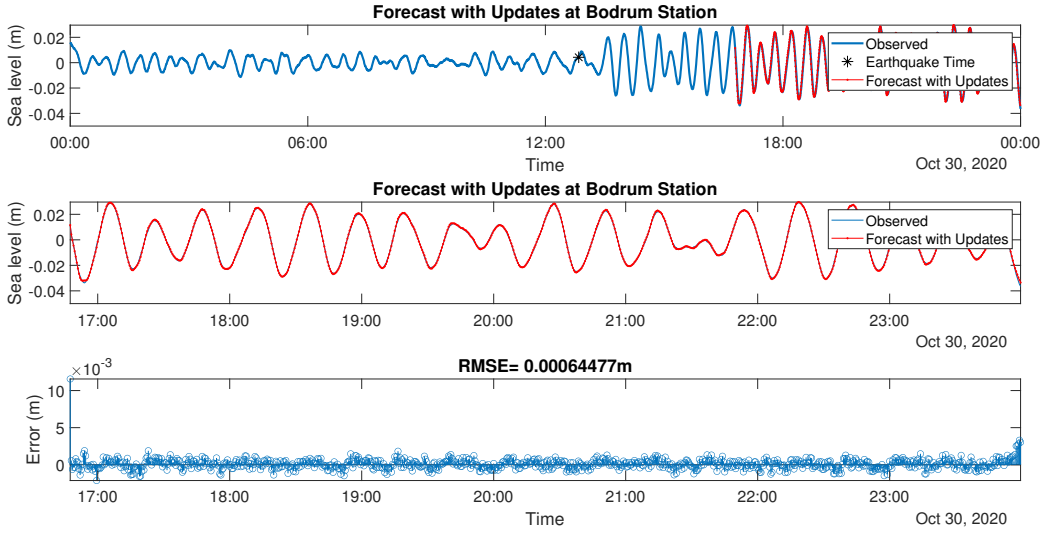

Figure 5. Time series of the İzmir-Samos tsunami water surface fluctuation recorded at Bodrum station [29] on 30 October 2020 and its prediction by LSTM DL network-with updates.

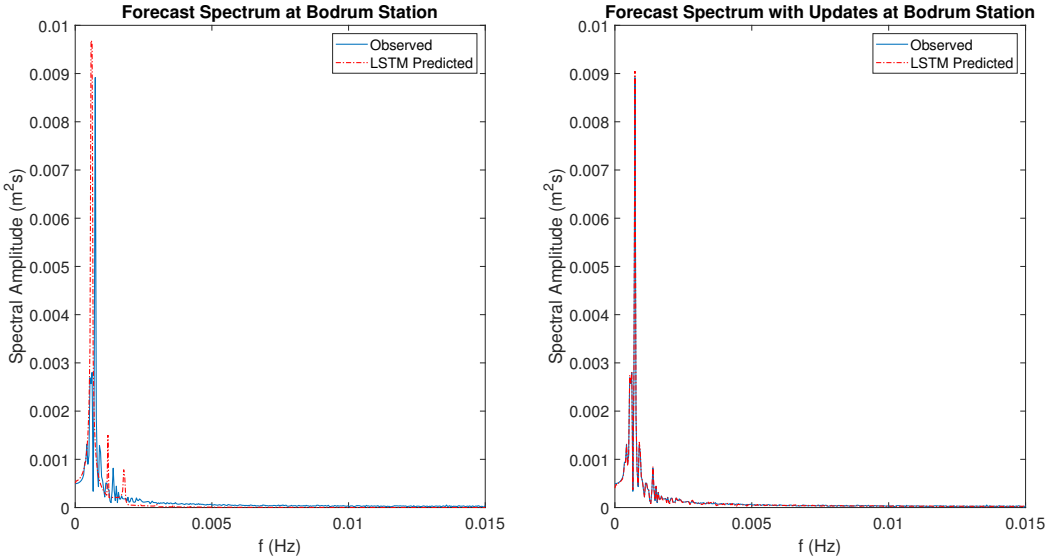

Figure 6. Comparison of Fourier spectra of time series predictions performed by LSTM DL network at Bodrum Station on 30 October 2020 (**left**) without updates (**right**) with updates.

In Figure 7, we present the recorded water surface elevation time series of the 30 October 2020 Tsunami at the Syros station and its prediction with the LSTM DL network with no updates. The same predictions with the updated LSTM network are presented in Figure 8. Comparing Figures 7 and 8 it is possible to realize that again LSTM predictions become significantly better when an updated network is used. Better performance can be observed by checking the RMSE as well as the comparisons of the spectra depicted in Figures 9 and 10.

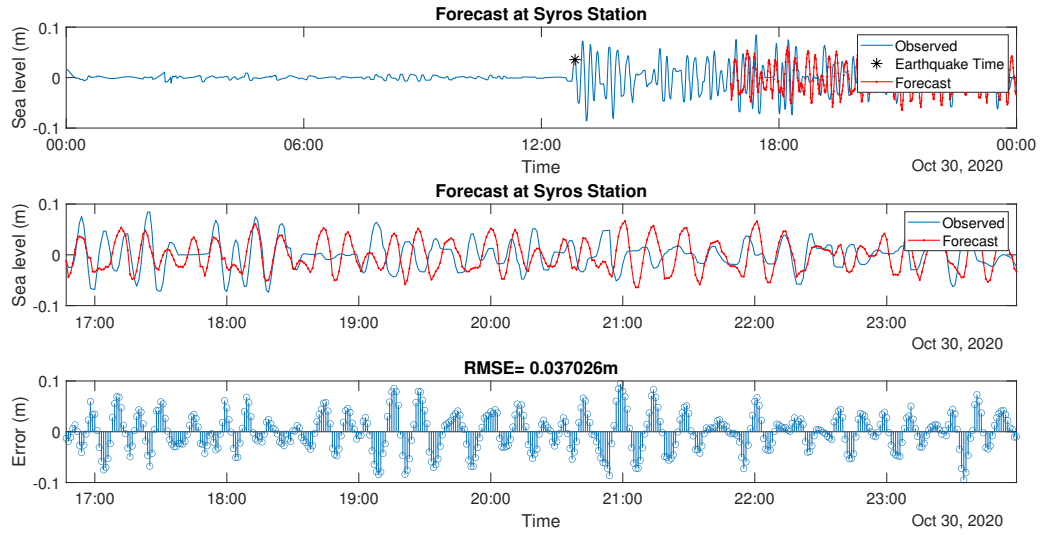

Figure 7. Time series of the İzmir-Samos tsunami water surface fluctuation recorded at Syros station [29] on 30 October 2020 and its prediction by LSTM DL network-without updates.

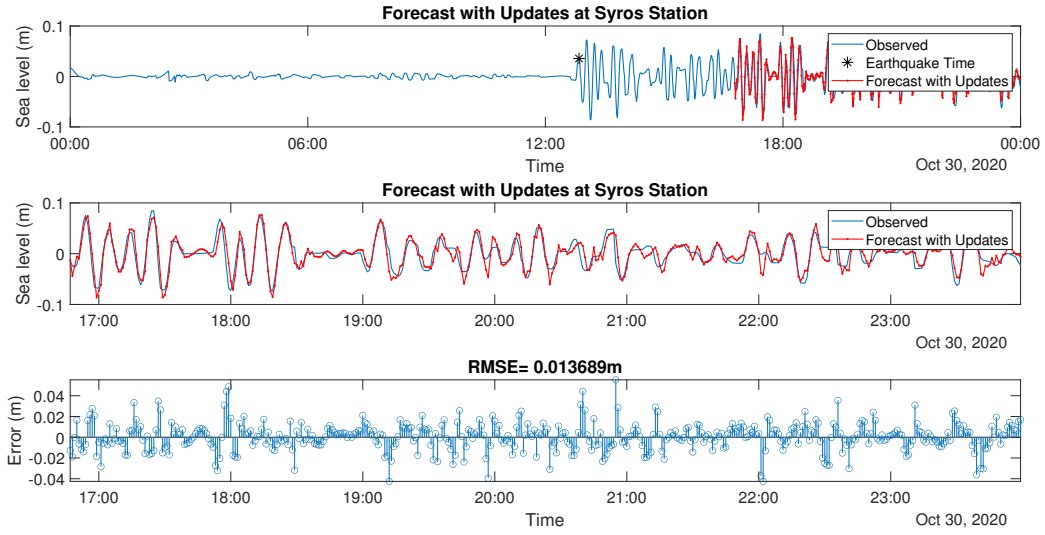

Figure 8. Time series of the İzmir-Samos tsunami water surface fluctuation recorded at Syros station [29] on 30 October 2020 and its prediction by LSTM DL network-with updates.

It is interesting and useful to recognize that LSTM with updates is more successful in predicting the lower frequency components for the tsunami time series recorded at Syros station, however, for higher frequency components (shorter waves) an increase in the mismatch of the spectral amplitudes can be observed. One possible way to minimize such effects is to develop an LSTM DL network with some frequency band filters using FFT or similar routines.

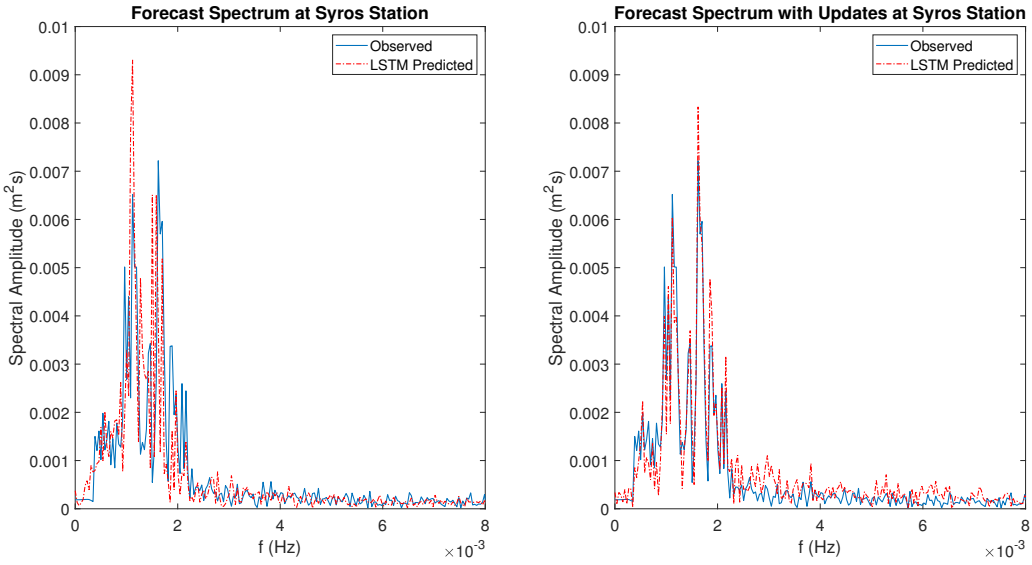

Figure 9. Comparison of Fourier spectra of time series predictions performed by LSTM DL network at Syros station on 30 October 2020 (**left**) without updates (**right**) with updates.

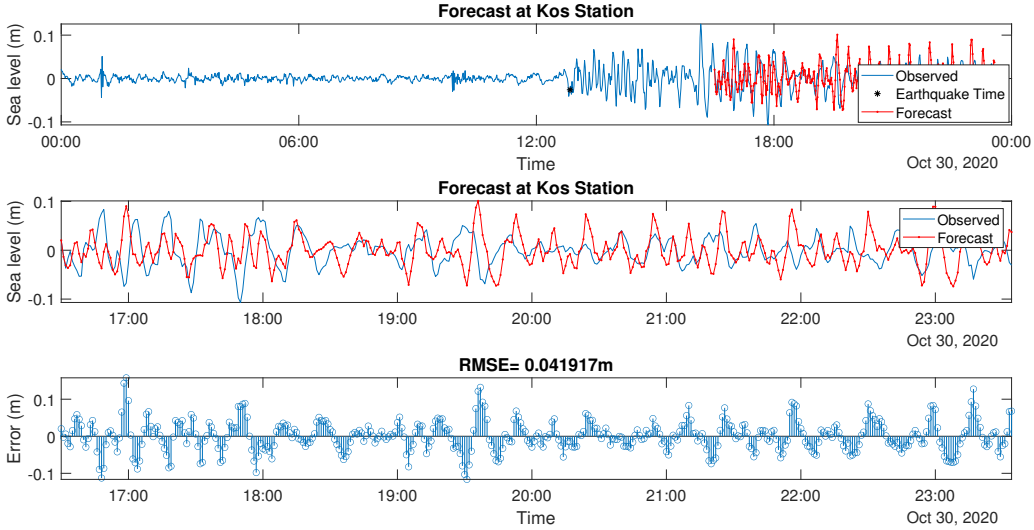

Figure 10. Time series of the İzmir-Samos tsunami water surface fluctuation recorded at Kos station [29] on 30 October 2020 and its prediction by LSTM DL network-without updates.

The similar prediction analysis for the tsunami time series recorded at Kos station located at [latitude: 36.898362, longitude: 27.287792] is repeated the results obtained using the LSTM network with no updates are depicted in Figure 11. The maximum tsunami wave height in this time series was recorded to be around 20cm which remains in the training data part, for the predicted part it is around 16cm as time series depicted in Figure 11 and one-sided (half-amplitude) Fourier spectra depicted in Figure 12 confirms. The highest RMSE among all data sets is depicted in Figure 11, mainly due to phase mismatch between actual recordings and predictions. It can be observed that the spectral features of the Kos station time series differ from their counterparts analyzed before. Some of the reasons for this fact are the recordings are carried out by radar which is more sensitive compared to pressure gauge, as well as tsunami asymptotics can change with barriers and distance [3].

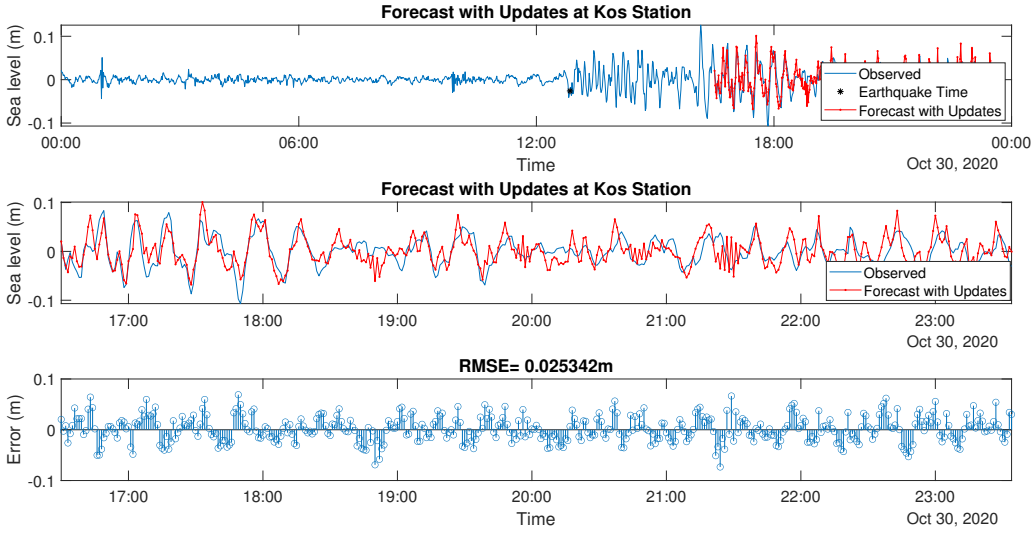

Figure 11. Time series of the İzmir-Samos tsunami water surface fluctuation recorded at Kos station [29] on 30 October 2020 and its prediction by LSTM DL network-with updates.

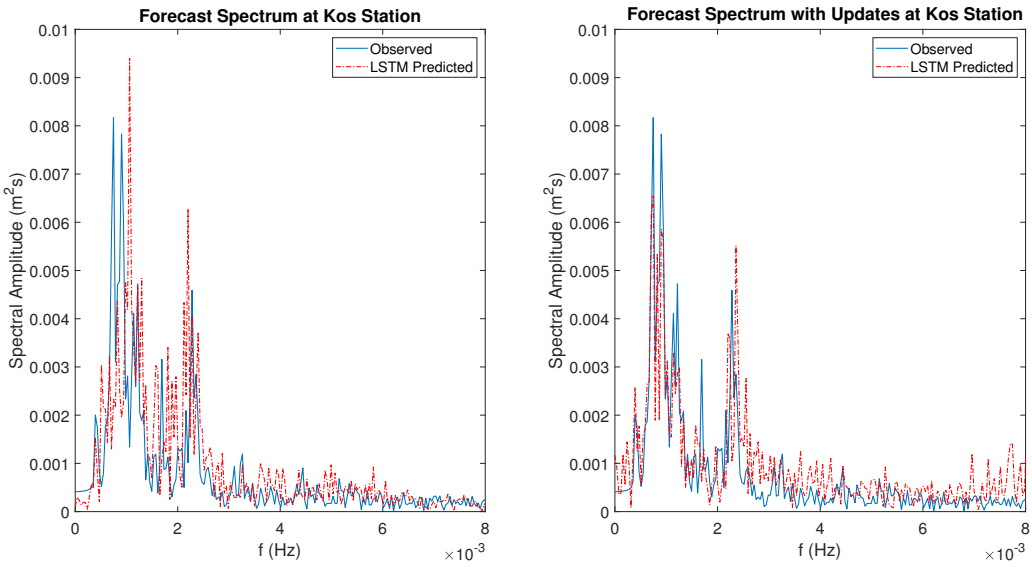

Figure 12. Comparison of Fourier spectra of time series predictions performed by LSTM DL network at Kos Station on 30 October 2020 (**left**) without updates (**right**) with updates.

It is again useful to observe that LSTM with updates leads to spectral amplitude mismatch at higher wavenumbers; however, it predicts the lower frequency components with higher amplitudes better, as before. This can lead to the development of filtered LSTM networks for the removal and isolation of such components.

The last data set analyzed is recorded at the Kos Marina station located at [latitude: 36.891013, longitude: 27.303632] which is very close to the Kos station mentioned above. Similarly, the maximum tsunami wave height in this time series was recorded to be around 20 cm which remains in the training data part, for the predicted part it is around 14 cm as the time series depicted in Figure and one-sided (half-amplitude) Fourier spectra depicted in Figure confirms. The highest RMSE among all data sets is depicted in Figure 11, mainly due to phase mismatch between actual recordings and predictions. The characteristics of the time series are more similar to the time series recorded at the Kos station discussed above.

Figures 13–15 confirm that prediction by the LSTM network with no updates is better compared to the case of Kos station, however, a similar high wavenumber spectral amplitude mismatch pattern can still be observed. Again, such features may be suppressed by using spectral filters to allow for specific bandwidth of predictions.

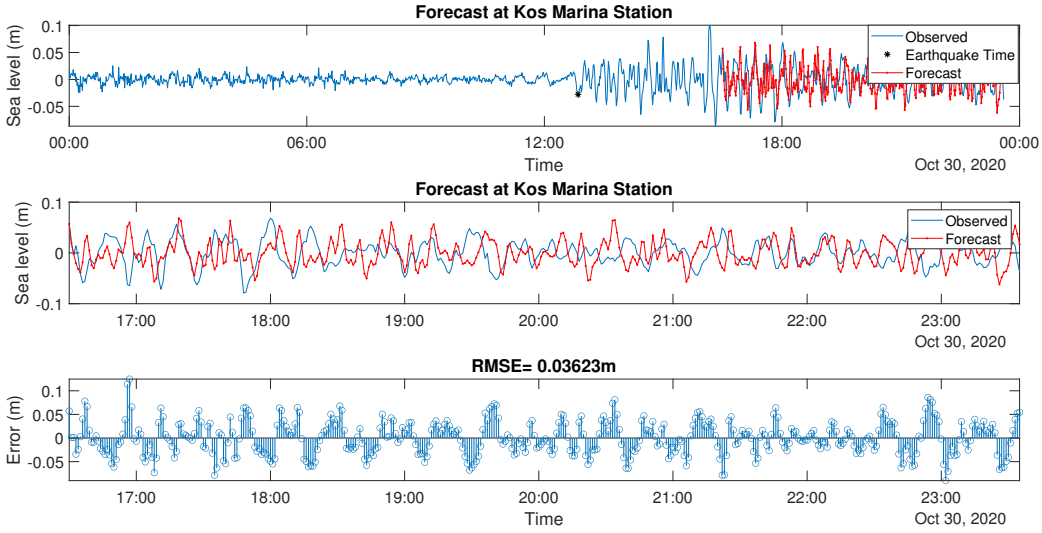

Figure 13. Time series of the İzmir-Samos tsunami water surface fluctuation recorded at Kos Marina station [29] on 30 October 2020 and its prediction by LSTM DL network-without updates.

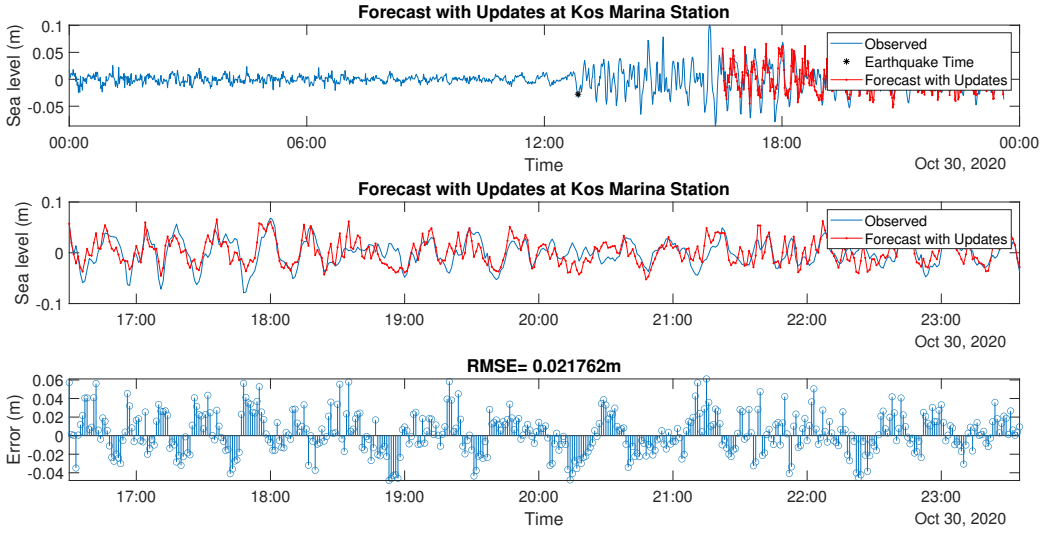

Figure 14. Time series of the İzmir-Samos tsunami water surface fluctuation recorded at Kos Marina station [29] on 30 October 2020 and its prediction by LSTM DL network-with updates.

Lastly, we turn our attention to the analysis of the effect of the length of the training data set on prediction results. For all the simulations reported above, we use 70% of the daily tsunami time series to predict the remaining 30%. The training data set includes both the pre-earthquake and post-earthquake recordings. Now, as an illustrative example we set the length of the training data set to be 85% of the daily tsunami time series recorded at the Kos Marina, thus re-perform the last analysis with these values.

Checking Figures 16–18 and comparing them with Figures 13–15, one can realize that increasing the length of training data has a significant effect on reducing RMSE error and

phase mismatch, however, in our simulations, we observe that although this is generally the case, there is not always a monotonic relation. Thus, the training data set must be selected with care. Additionally, by comparing the Fourier spectra of the last two analyses, one can realize that spectral amplitude mismatch between observations and predictions at higher wavenumbers is unlikely to be reduced by increasing the length of the training data set. Thus, a filtering approach may be developed.

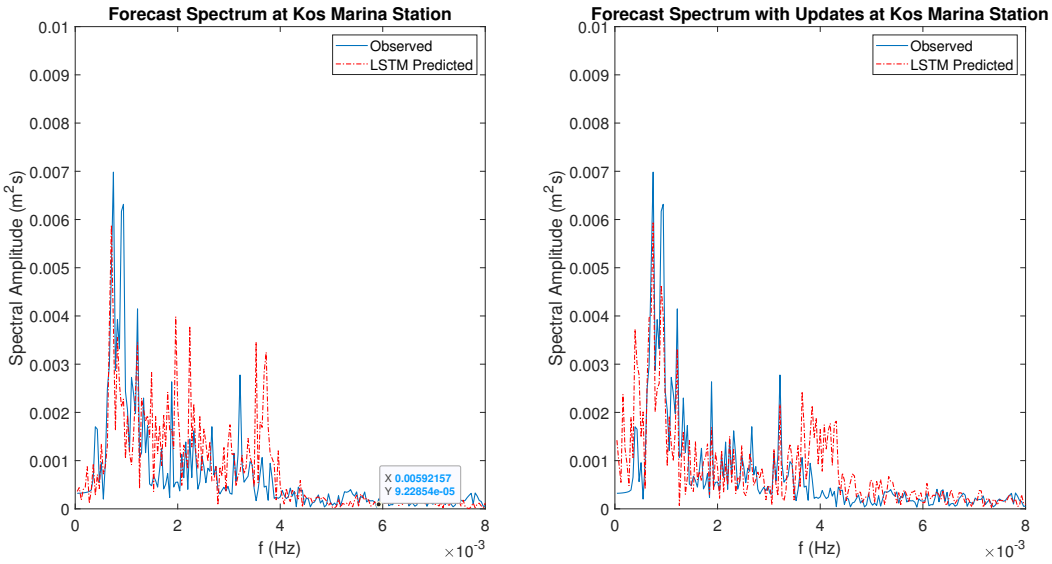

Figure 15. Comparison of Fourier spectra of time series predictions performed by LSTM DL network at Kos Marina Station on 30 October 2020 (**left**) without updates (**right**) with updates.

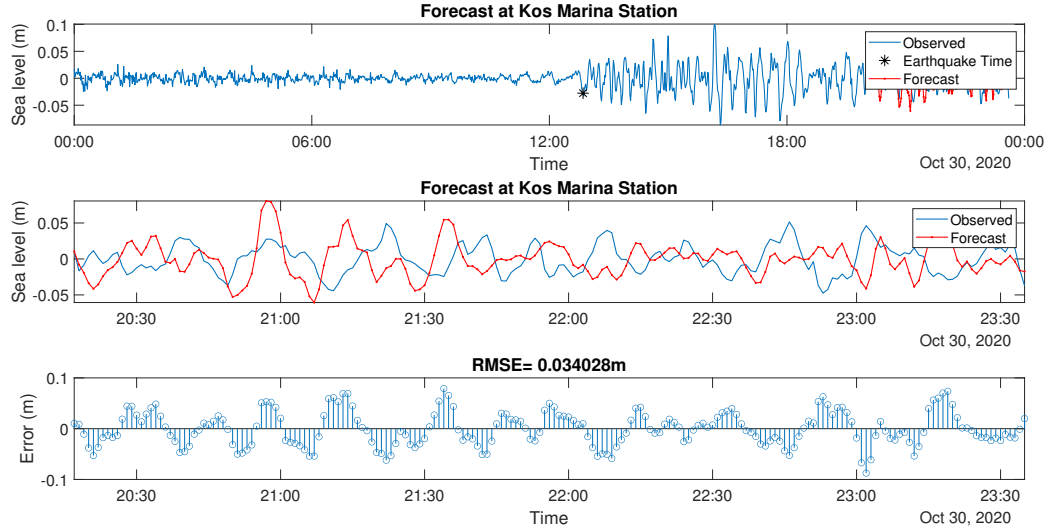

Figure 16. Time series of the İzmir-Samos tsunami water surface fluctuation recorded at Kos Marina station [29] on 30 October 2020 and its prediction by LSTM DL network using 85% training data-without updates.

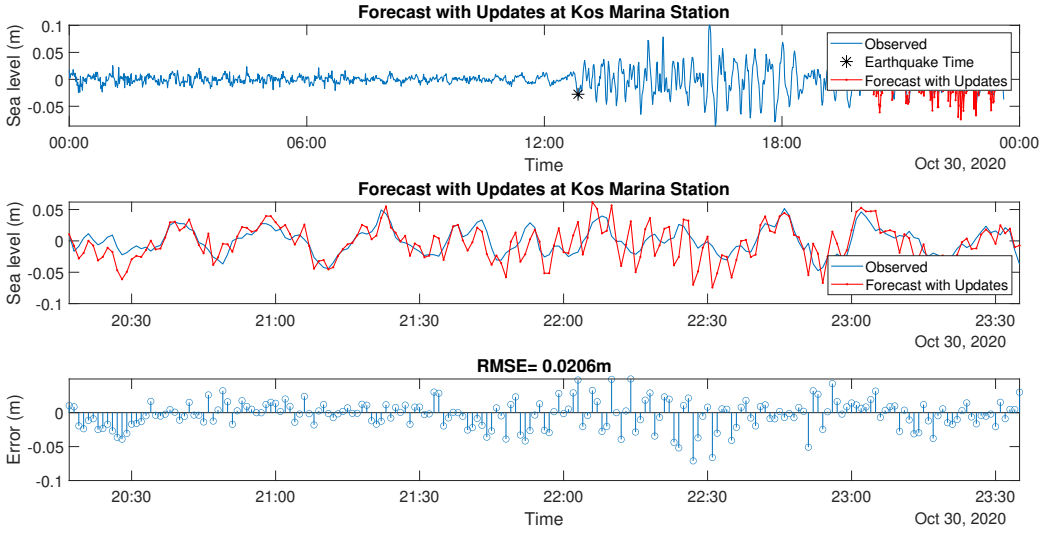

Figure 17. Time series of the İzmir-Samos tsunami water surface fluctuation recorded at Kos Marina station [29] on 30 October 2020 and its prediction by LSTM DL network using 85% training data-with updates.

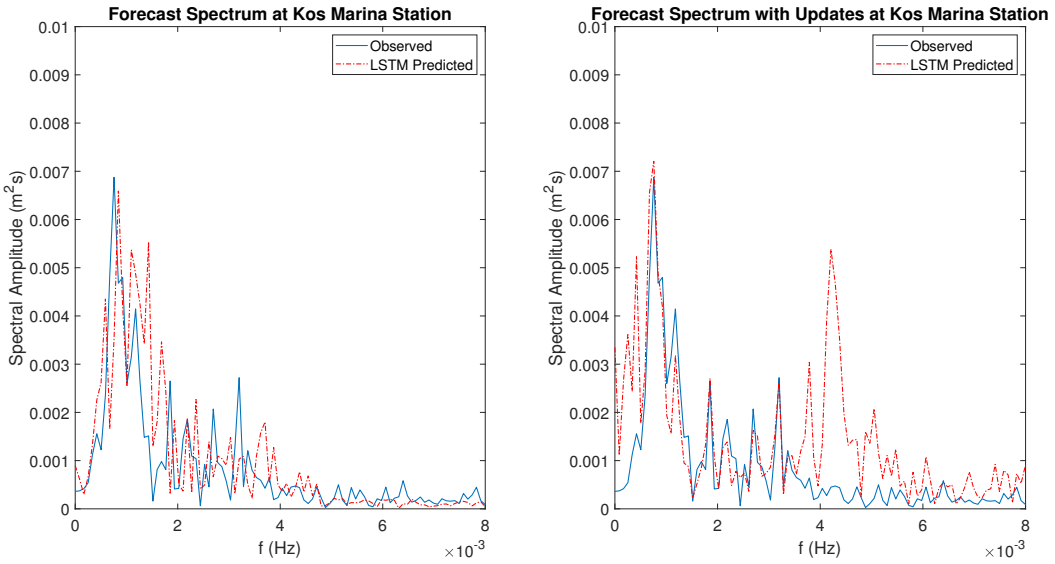

Figure 18. Comparison of Fourier spectra of time series predictions performed by LSTM DL network using 85% training data at Kos Marina Station on 30 October 2020 (**left**) without updates (**right**) with updates.

The results of our paper are promising to enhance the predictions of tsunami events and hydrodynamics. Even when the LSTM network with updates is used, although the predictions are valid for a one-time step, the time steps investigated in this paper are either 0.5 min or 1 min. Such time scales can be quite beneficial to save lives and avoiding damage and loss by more precise mapping of possible tsunami inundation and run-up time series, which exhibit nonlinear features that can be modeled using nonlinear equations such as those in [3,32]. Besides this, there are many different tsunami early warning systems [33]. The majority of these systems rely on techniques such as measuring and estimating the tsunamigenic potential of an earthquake using seismic data, or detection of Tsunami Waves using Sea-level Networks after a tsunami occurs in deep water. Bottom pressure recorders, coastal tide-gauge stations, current meters, buoys, or radars are used for

the latter systems [33]. According to the National Oceanic and Atmospheric Administration (NOAA), the early warning time scale for tsunamis ranges from five minutes to two hours, depending on the distance between its source and the nearest Deep-ocean Assessment and Reporting of Tsunami (DART) system or coastal water-level station. Such time scales can be significantly developed (same order of magnitude) using the proposed methodology in this paper, which depends on LSTM or similar DL networks. Also, not only the early warning time scales would be enhanced using our findings, but also more accurate predictions of tsunami hydrodynamic parameters such as water surface level, run-up, or run-up volume can be made [34,35].

4. Conclusions

In this article, we have looked at the potential application of the LSTM deep learning network for predicting tsunami hydrodynamics. For this purpose, we analyzed the daily water surface fluctuation time series data of the 30 October 2020 İzmir-Samos Tsunami recorded at various UNESCO stations. We have demonstrated that a successful prediction of such a time series using LSTM, both with and without updates, is possible. Even only utilizing an LSTM network without updates produced good results especially for the Bodrum station, we demonstrated that the LSTM with updates is more successful and consistent in prediction. Prediction time scale of the post-event accurate hydrodynamics are on the order of a few hours for the case with no updates, however, when an updated network is used it is restricted to one time step which is either 0.5 min or 1 min for the data investigated in this paper. We have also discussed the spectral features of the predictions, showing that although some mismatch at higher frequencies can be observed, the LSTM network can predict the tsunami time series spectrum reasonably well.

Our findings can be used to enhance tsunami early warning times on the order of minutes to hours depending on the location and size of the event. This feature would be especially helpful when the event at an offshore location is detected. After the recording of the event, secondary waves and tsunami asymptotics can be predicted at the offshore stations, thus the early warning time scale can be enhanced for the coastal regions and more accurate mapping of the inundation at the shore can be performed. Also, our results can be easily extended to predict tsunami parameters such as the horizontal and excursion velocities, and run-up time series. In the near future, we plan to extend our findings to other DL networks and time series prediction tools such as compressive sensing of nonlinear processes [36,37]. Additionally, tsunami run-up, inundation characteristics, as well as the determination of seismic behavior using tsunami data, will be investigated using the DL and some other AI techniques, where other observational data or analytical/numerical approaches such as the one discussed in [38] can be utilized.

Author Contributions: Conceptualization, C.B. and A.R.A.; methodology, A.R.A., C.B. and F.O.; software, C.B., A.R.A., F.O. and A.A.A.; validation, A.R.A. and C.B.; formal analysis, C.B. and A.R.A.; investigation, C.B., A.A.A. and F.O.; resources, A.R.A. and C.B.; writing—original draft preparation, A.R.A. and C.B.; visualization, A.R.A. and C.B.; supervision, C.B., F.O. and A.A.A.; funding acquisition, C.B. All authors have read and agreed to the published version of the manuscript.

Funding: This study is funded by the Turkish Academy of Sciences (TÜBA)-Outstanding Young Scientist Award (GEBİP), and the Research Fund of the Istanbul Technical University with project codes: MGA-2022-43528, MDK-2021-42849 and by the Personal Research Fund of Tokyo International University.

Institutional Review Board Statement: Not applicable.

Informed Consent Statement: Not applicable.

Data Availability Statement: All the results can be reproduced through the presented methods.

Acknowledgments: The authors are grateful to Doğan Kalafat for giving permission for the reuse of Figure 1.

Conflicts of Interest: The authors declare no conflict of interest.

Abbreviations

The following abbreviations are used in this manuscript:

AI	Artifical Intelligence
DART	Deep-ocean Assessment and Reporting of Tsunami
DL	Deep Learning
FFT	Fast Fourier Transform
GMT	Greenwich Mean Time
IFFT	Inverse Fast Fourier Transform
KOERI	Boğaziçi University Kandilli Observatory and Earthquake Research Institute
LSTM	Long-short term memory
NOAA	National Oceanic and Atmospheric Administration
RMSE	Root Mean Square Error
RNN	Recurrent Neural Networks
UTC	Universal Time Coordinated

References

1. Ward, S.N. Tsunamis. *Encycl. Phys. Sci. Technol.* **2001**, *17*, 175–191.
2. Chapman, C. The Asian tsunami in Sri Lanka: A personal experience. *EOS Trans. Am. Geophys. Union* **2005**, *86*, 13–14. [CrossRef]
3. Berry, M.V. Tsunami asymptotics. *New J. Phys.* **2005**, *7*, 129. [CrossRef]
4. Röbke, B.; Vött, A. The tsunami phenomenon. *Prog. Oceanogr.* **2017**, *159*, 296–322. [CrossRef]
5. Ishihara, M.; Tadono, T. Land cover changes induced by the great east Japan earthquake in 2011. *Sci. Rep.* **2017**, *7*, 45769. [CrossRef] [PubMed]
6. Kaiser, G.; Burkhard, B.; Römer, H.; Sangkaew, S.; Graterol, R.; Haitook, T.; Sterr, H.; Sakuna-Schwartz, D. Mapping tsunami impacts on land cover and related ecosystem service supply in Phang Nga, Thailand. *Nat. Hazards Earth Syst. Sci.* **2013**, *13*, 3095–3111. [CrossRef]
7. Richmond, B.; Szczuciński, W.; Chagué-Goff, C.; Goto, K.; Sugawara, D.; Witter, R.; Tappin, D.R.; Jaffe, B.; Fujino, S.; Nishimura, Y.; et al. Erosion, deposition and landscape change on the Sendai coastal plain, Japan, resulting from the March 11, 2011 Tohoku-oki tsunami. *Sediment. Geol.* **2012**, *282*, 27–39. [CrossRef]
8. Tappin, D.R.; Evans, H.M.; Jordan, C.J.; Richmond, B.; Sugawara, D.; Goto, K. Coastal changes in the Sendai area from the impact of the 2011 Tōhoku-oki tsunami: Interpretations of time series satellite images, helicopter-borne video footage and field observations. *Sediment. Geol.* **2012**, *282*, 151–174. [CrossRef]
9. Bayındır, C. Analysis of tsunami and tsunami-structure interaction parameters by compressive sensing. In Proceedings of the ICAME'21, Balıkesir, Turkey, 1–3 September 2021; p. 25.
10. Sambah, A.B.; Miura, F. Remote sensing, GIS, and AHP for assessing physical vulnerability to tsunami hazard. *Int. J. Environ. Ecol. Eng.* **2013**, *7*, 671–679. [CrossRef]
11. Yamazaki, F.; Matsuoka, M. Remote sensing technologies in post-disaster damage assessment. *J. Earthq. Tsunami* **2007**, *1*, 193–210. [CrossRef]
12. Dogan, G.G.; Yalciner, A.C.; Yuksel, Y.; Ulutas, E.; Polat, O.; Guler, I.; Sahin, C.; Tarih, A.; Kanoglu, U. The 30 October 2020 Aegean Sea Tsunami: Post-Event Field Survey Along Turkish Coast. *Pure Appl. Geophys.* **2021**, *178*, 785–812. [CrossRef] [PubMed]
13. Triantafyllou, I.; Gogou, M.; Mavroulis, S.; Lekkas, E.; Papadopoulos, G.A.; Thravalos, M. The tsunami caused by the 30 October 2020 Samos (Aegean Sea) Mw7.0 earthquake: Hydrodynamic features, source properties and impact assessment from post-event field survey and video records. *J. Mar. Sci. Eng.* **2021**, *9*, 68. [CrossRef]
14. Evelpidou, N.; Karkani, A.; Kampolis, I. Relative sea level changes and morphotectonic implications triggered by the Samos earthquake of 30th October 2020. *J. Mar. Sci. Eng.* **2020**, *9*, 40. [CrossRef]
15. Politis, D.; Potirakis, S.; Contoyiannis, Y.; Biswas, S.; Sasmal, S.; Hayakawa, M. Statistical and criticality analysis of the lower ionosphere prior to the 30 October 2020 Samos (Greece) earthquake (M6.9), based on VLF electromagnetic propagation data as recorded by a new VLF/LF receiver installed in Athens (Greece). *Entropy* **2021**, *23*, 676. [CrossRef] [PubMed]
16. Mase, H.; Yasuda, T.; Mori, N. Real-time prediction of tsunami magnitudes in Osaka Bay, Japan, using an artificial neural network. *J. Waterw. Port Coast. Ocean. Eng.* **2011**, *137*, 263–268. [CrossRef]
17. Mitra, R.; Naruse, H.; Abe, T. Estimation of tsunami characteristics from deposits: Inverse modeling using a deep-learning neural network. *J. Geophys. Res. Earth Surf.* **2020**, *125*, e2020JF005583. [CrossRef]
18. Makinoshima, F.; Oishi, Y.; Yamazaki, T.; Furumura, T.; Imamura, F. Early forecasting of tsunami inundation from tsunami and geodetic observation data with convolutional neural networks. *Nat. Commun.* **2021**, *12*, 2253. [CrossRef]
19. Fauzi, A.; Mizutani, N. Machine learning algorithms for real-time tsunami inundation forecasting: A case study in Nankai region. *Pure Appl. Geophys.* **2020**, *177*, 1437–1450. [CrossRef]
20. Mulia, I.E.; Ueda, N.; Miyoshi, T.; Gusman, A.R.; Satake, K. Machine learning-based tsunami inundation prediction derived from offshore observations. *Nat. Commun.* **2022**, *13*, 5489. [CrossRef]

21. Wang, Y.; Imai, K.; Miyashita, T.; Ariyoshi, K.; Takahashi, N.; Satake, K. Coastal tsunami prediction in Tohoku region, Japan, based on S-net observations using artificial neural network. *Earth Planets Space* **2023**, *75*, 154. [CrossRef]
22. Xu, H.; Wu, H. Accurate Tsunami Wave Prediction Using Long Short-term Memory Based Neural Networks. *Ocean Model.* **2023**, *186*, 102259. [CrossRef]
23. Dharmawan, W.; Diana, M.; Tuntari, B.; Astawa, I.M.; Rahardjo, S.; Nambo, H. Tsunami tide prediction in shallow water using recurrent neural networks: Model implementation in the Indonesia Tsunami Early Warning System. *J. Reliab. Intell. Environ.* **2023**. [CrossRef]
24. Geiß, C.; Maier, J.; So, E.; Schoepfer, E.; Harig, S.; Gomez Zapata, J.C.; Zhu, Y. Anticipating a risky future: LSTM models for spatiotemporal extrapolation of population data in areas prone to earthquakes and tsunamis in Lima, Peru. *EGUsphere* **2023**. [CrossRef]
25. Kiratzi, A.; Papazachos, C.; Özacar, A.; Pinar, A.; Kkallas, C.; Sopaci, E. Characteristics of the 2020 Samos earthquake (Aegean Sea) using seismic data. *Bull. Earthq. Eng.* **2022**, *20*, 7713–7735. [CrossRef]
26. Sboras, S.; Lazos, I.; Bitharis, S.; Pikridas, C.; Galanakis, D.; Fotiou, A.; Chatzipetros, A.; Pavlides, S. Source modelling and stress transfer scenarios of the October 30, 2020 Samos earthquake: Seismotectonic implications. *Turk. J. Earth Sci.* **2021**, *30*, 699–717. [CrossRef]
27. Ren, C.; Yue, H.; Cao, B.; Zhu, Y.; Wang, T.; An, C.; Ge, Z.; Li, Z. Rupture process of the 2020 Mw = 6.9 Samos, Greece earthquake on a segmented fault system constrained from seismic, geodetic, and tsunami observations. *Tectonophysics* **2022**, *839*, 229497. [CrossRef]
28. KOERI. Boğaziçi University Kandilli Observatory and Earthquake Research Institute, Regional Earthquake-Tsunami Monitoring and Evaluation Center 30 October 2020 Aegean Sea Earthquake Press Release. 2020. Available online: http://www.koeri.boun.edu.tr/sismo/2/wp-content/uploads/2020/10/20201030_izmir_V1.pdf (accessed on 10 October 2023).
29. UNESCO/IOC. UNESCO Intergovernmental Oceanographic Commission Sea Level Station Monitoring Facility. 2020. Available online: https://www.ioc-sealevelmonitoring.org/station.php?code=stationcode (accessed on 10 October 2023).
30. Hochreiter, S.; Schmidhuber, J. Long short-term memory. *Neural Comput.* **1997**, *9*, 1735–1780. [CrossRef]
31. Olah, C. Understanding LSTM Networks. 2015. Available online: https://colah.github.io/posts/2015-08-Understanding-LSTMs/ (accessed on 10 October 2023).
32. Bayındır, C.; Altintas, A.A.; Ozaydin, F. Self-localized solitons of a q-deformed quantum system. *Commun. Nonlinear Sci. Numer. Simul.* **2021**, *92*, 105474. [CrossRef]
33. Srinivasa Kumar, T.; Manneela, S. A review of the progress, challenges and future trends in tsunami early warning systems. *J. Geol. Soc. India* **2021**, *97*, 1533–1544. [CrossRef]
34. González, F.I.; Milburn, H.; Bernard, E.; Newman, J. *Deep-Ocean Assessment and Reporting of Tsunamis (DART): Brief Overview and Status Report*; Technical Report; National Data Buoy Center: Bay Saint Louis, MS, USA, 2003.
35. Meinig, C.; Eble, M.C.; Stalin, S.E. *System Development and Performance of the Deep-Ocean Assessment and Reporting of Tsunamis (DART) System from 1997–2001*; Technical Report; NOAA Pacific Marine Environmental Laboratory: Seattle, WA, USA, 2001.
36. Bayındır, C.; Namli, B. Efficient sensing of Von Karman vortices using compressive sensing. *Comput. Fluids* **2021**, *226*, 104975. [CrossRef]
37. Bayındır, C. Compressive spectral renormalization method. *TWMS J. Appl. Eng. Math.* **2018**, *8*, 425–437.
38. Bueler-Faudree, T.; Sam, D.; Dutykh, D.; Rybkin, A.; Suleimani, A. Fast shallow water-wave solver for plane inclined beaches. *SoftwareX* **2021**, *17*, 100983. [CrossRef]